JOURNAL OF SOLID STATE CHEMISTRY 74, 369–376 (1988)

Defect Structure and Electrical Properties of Magnesium-Substituted Strontium Titanate

OM PARKASH* AND CH. DURGA PRASAD

School of Materials Science and Technology, Institute of Technology, Banaras Hindu University, Varanasi 221 005, India

AND DEVENDRA KUMAR

Department of Ceramic Engineering, Institute of Technology, Banaras Hindu University, Varanasi 221 005, India

Received July 20, 1987; in revised form October 21, 1987

Attempts were made to synthesize samples in the system $SrTi_{1-x}Mg_xO_3$ for $x = 0.01, 0.05, 0.10, 0.15, 0.20$, and 0.25. Solid solution is obtained in the compositions with $x \leq 0.10$. The structure remains cubic. Chemical analysis indicates oxygen deficiency in these materials. Initial substitution of Mg^{2+} ions (i.e., for $x = 0.01$) lowers the resistivity by several orders of magnitude. The activation energy, E_a, is very small and AC conductivity is independent of frequency in this composition. At higher concentration of Mg^{2+} ions (i.e., for $x = 0.05$ and 0.10), the resistivity and the activation energy again increases. AC conductivity, σ_{AC}, varies as ω^s where s lies in the range 0.4–0.6, indicating conduction by hopping of charge carriers. The dielectric constant of these samples remains constant up to a particular temperature, T_c, beyond which it varies as $A(T - T_c)/\omega^{s'}$. The electrical behavior has been explained on the basis of the defect structure of these materials.

Introduction

Strontium titanate is an ABO_3-type perovskite which is paraelectric at room temperature. Substitution of higher valent ions on A and B sites imparts interesting dielectric properties to the resulting materials (*1–5*). By suitable heat treatment in a controlled atmosphere, rare-earth substituted $SrTiO_3$ becomes a potential candidate for boundary layer capacitors (*6–7*). The Mg^{2+} ion, when substituted in $SrTiO_3$, will replace the Ti^{4+} ion because of similar size. It will act as an acceptor on the B site being a lower valent ion than the Ti^{4+}. Electrical charge neutrality is expected to be achieved by oxygen vacancies (*8*). In this paper we report the results of our investigations on the possibility of formation of the solid solution $SrTi_{1-x}Mg_xO_3$ and the effect of its defect structure on the electrical properties.

Experimental

All the samples were prepared from analytical grade strontium oxalate, titanium dioxide, and magnesium oxide. Stoichiometric amounts of these materials were

* To whom all correspondence should be addressed.

0022-4596/88 $3.00

weighed, mixed, and ground. The dry powders were calcined at 1475 K for 6 hr. The resulting mass was mixed and ground again. Pellets were prepared using polyvinyl alcohol as binder. These pellets were slowly heated to 675 K, kept there for an hour to completely remove binder and then the temperature was raised to 1525 K at the rate of 150 K/hr. Samples were sintered at this temperature for 12 hr and cooled in the furnace. X-ray diffraction patterns were taken using an Isodebyeflex 2002 diffractometer employing Cu$K\alpha$ radiation. Chemical analysis was carried out using a Perkin–Elmer atomic absorption spectrophotometer. Bulk density of sintered pellets was determined by the water displacement method as well as from the geometry and mass of the pellets. Both values were identical. Porosity was calculated by the relation

$$\% \text{ Porosity} = \frac{\text{X-ray density} - \text{Bulk density}}{\text{X-ray density}} \times 100.$$

For measurement of the DC resistivity and the Seebeck coefficient as a function of temperature, sintered pellets were polished and pressed between spring-loaded platinum foils. These measurements were carried out using a Keithley 616 digital electrometer. AC conductivity and dielectric constant were measured on pellets coated with silver paint using an HP 4192A LF impedance analyzer as a function of frequency at different temperatures.

Results and Discussion

Structure

$SrTiO_3$ is an ABO_3-type perovskite. X-ray diffraction (XRD) data indicate that the Mg^{2+} ion has limited solubility in $SrTiO_3$. Solid solution is formed only in the compositions with $x = 0.01$, 0.05, and 0.10 studied by us. XRD patterns of the compositions with $x = 0.15$, 0.20 and 0.25 were found to contain characteristic lines of the constituent oxides. Firing of these compositions even at 1623 K did not give single-phase materials. We have characterized compositions with values of $x = 0.01$, 0.05, and 0.10 which are single-phase materials. Data on $SrTiO_3$ prepared by us is also given for comparison. Chemical analysis of these samples indicate that they are oxygen deficient similar to the system $SrZr_{1-x}Mg_xO_3$ (*9*). As expected, for each Mg^{2+} replacing Ti^{4+}, electrical neutrality is maintained by creation of an oxygen vacancy. Thus these materials can be represented by the formula $SrTi_{1-x}Mg_xO_{3-x}$. XRD data of these samples could be indexed on the basis of a cubic unit cell. Lattice parameter, a, and percentage porosity for the samples with $x = 0.01$, 0.05, and 0.10 are given in Table I. Lattice parameter, a, does not change with x. This is because ionic radius of Mg^{2+} (0.72 Å) is larger than that of Ti^{4+} (0.61 Å). Replacement of Ti^{4+} by Mg^{2+} tends to increase a. On the other hand, the presence of oxygen vacancies tends to shrink the unit cell. The concentration of oxygen vacancies increases with concentration of Mg^{2+} ions. Thus these two effects cancel each other and the lattice parameter does not change with x. It is seen from Table I that percentage porosity increases with increasing x. The observed decrease in sinterability is in

TABLE I

LATTICE PARAMETER, a (Å), AND PERCENTAGE POROSITY FOR VARIOUS COMPOSITIONS IN THE SYSTEM $SrTi_{1-x}Mg_xO_{3-x}$

x	a (Å)	% Porosity
0.00	3.902	9.0
0.01	3.909	7.5
0.05	3.898	11.8
0.10	3.901	18.5

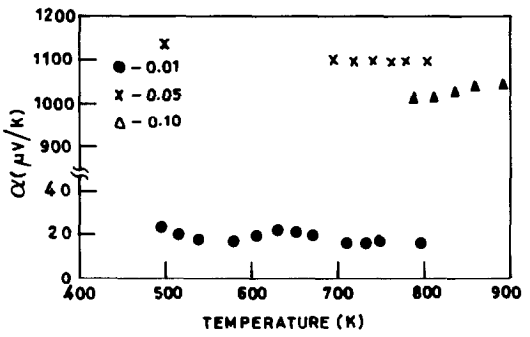

FIG. 1. Plots of Seebeck coefficient α vs temperature for the system $SrTi_{1-x}Mg_xO_{3-x}$.

accordance with the increase in oxygen vacancies which are reported to inhibit the sintering in the perovskite oxides (*8*).

Electrical Conductivity Behavior

All the samples exhibit time-independent DC conductivity over the entire range of temperatures of measurement. This shows that the conduction is predominantly electronic in nature. This behavior is similar to that observed in Mg^{2+}-doped $LaAlO_3$ and $SrZrO_3$ (*9*). The plots of Seebeck coefficient α as a function of temperature are shown in Fig. 1. Measurements of α below 800 K for the samples with $x = 0.05$ and 0.10 were not possible because of their high resistance. Positive values of α for all the samples show that the holes are majority charge carriers. The α is almost independent of temperature. The values of α at 800 K for all the samples are given in Table II.

TABLE II

SEEBECK COEFFICIENT, α, ACTIVATION ENERGY FOR DC CONDUCTIVITY, E_a, AC CONDUCTIVITY, E'_a, AND HOPPING ENERGY, W_1

x	α (μV/K) at 800 K	E_a (eV)	E'_a (eV) 10 kHz	E'_a (eV) 100 kHz	W_1 (eV)
0.01	16	0.13	—	—	—
0.05	1090	0.65	0.15	0.20	0.47
0.10	1010	0.62	0.16	0.16	0.46

Figure 2 shows the variation of log ρ_{DC} with $1000/T$ for all the compositions. It is clear from these plots that resistivity follows an Arrhenius relationship

$$\rho = \rho_0 \exp(E_a/kT), \qquad (1)$$

where E_a is the activation energy for conduction. Values of E_a determined from the slopes of these curves are given in Table II. Resistivity of the sample with $x = 0.01$ is 4–5 orders of magnitude less than that of Sr TiO_3. With further substitution, resistivity again starts increasing as indicated by plots of the $x = 0.05$ and $x = 0.10$ samples. Activation energy of conduction for $x = 0.01$ is also much less than that for the $x = 0.05$ and $x = 0.10$ samples, both of which have almost the same value. This shows that the conduction mechanism is different in the $x = 0.01$ sample from that operative in the other two samples.

$SrTiO_3$ is a p-type semiconductor. This is due to excess cation vacancies in A sublattice over oxygen vacancies similar to Ba TiO_3, i.e., it is cation deficient (*8*). These A site vacancies act as acceptors as they

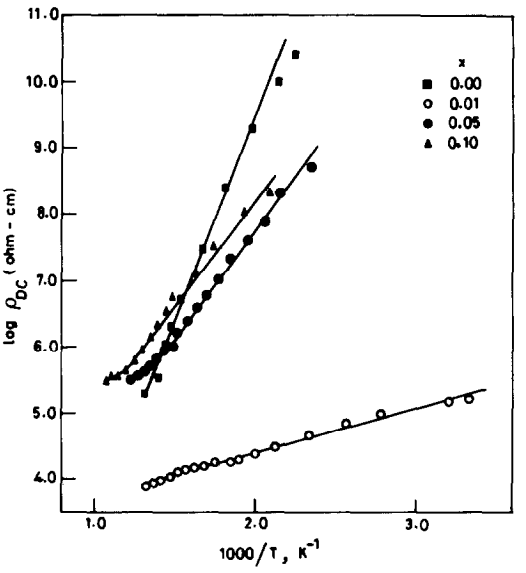

FIG. 2. Variation of log ρ_{DC} with $1000/T$ for the system $SrTi_{1-x}Mg_xO_{3-x}$.

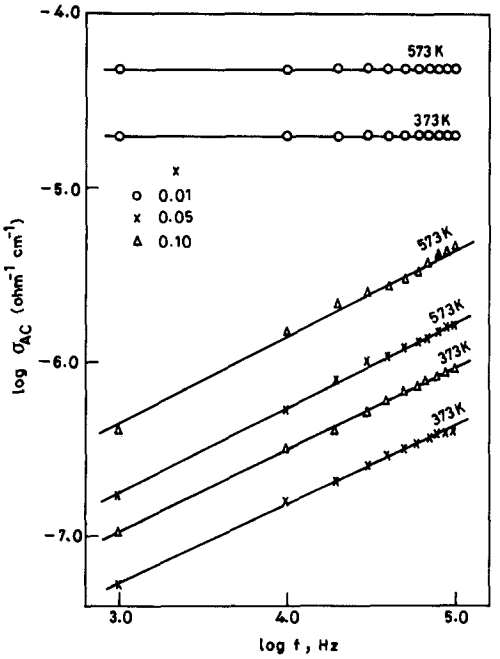

FIG. 3. Variation of log σ_{AC} with log f at different temperatures for the system $SrTi_{1-x}Mg_xO_{3-x}$.

attract electrons to complete the electron shells of the surrounding oxygen,

$$V_A \rightleftharpoons V_A^{--} + 2h^{\cdot}, \qquad (2)$$

generating holes, making $SrTiO_3$ a p-type semiconductor. Magnesium when substituted for titanium is short of two electrons to complete bonding with the surrounding oxygen ions. It can accept two electrons from the oxygen-2p valence band, thereby generating two holes in it. Initial substitution of magnesium, therefore, leads to generation of a large number of holes. Variation of AC conductivity, σ_{AC}, for all the samples with frequency at a few selected temperatures is shown in Fig. 3. For the sample with $x = 0.01$, σ_{AC} is independent of frequency at all temperatures. The temperature-independent value of Seebeck coefficient of this sample shows that the number of charge carriers remains constant with the temperature. Therefore, the electrical conduction seems to occur by the hopping of small polarons among localized defect sites. The activation energy for conduction is entirely due to thermally activated mobility of small polarons (*10, 11*).

The frequency dependence of AC conductivity, $\sigma_{AC}(\omega)$, for the samples with $x = 0.05$ and 0.10 (Fig. 3) can be expressed as

$$\sigma_{AC}(\omega) \alpha \omega^s, \qquad (3)$$

where s is a weak function of frequency at a particular temperature. It has a value in the ranges 0.45–0.52 and 0.40–0.62 for the samples with $x = 0.05$ and 0.10, respectively in the temperature range 300–575 K. Value of s increases with temperature. Plots of log σ_{AC} vs $1000/T$ at a few frequencies (1, 10, and 100 kHz) are shown in Fig. 4 for these two compositions. It is observed that these plots are linear above 350 K. The values of activation energy, E_a', calculated from the slopes are given in Table II.

The frequency dependence of AC conductivity can arise due to the following mechanisms: (i) transport by carriers excited into localized states at the band edge,

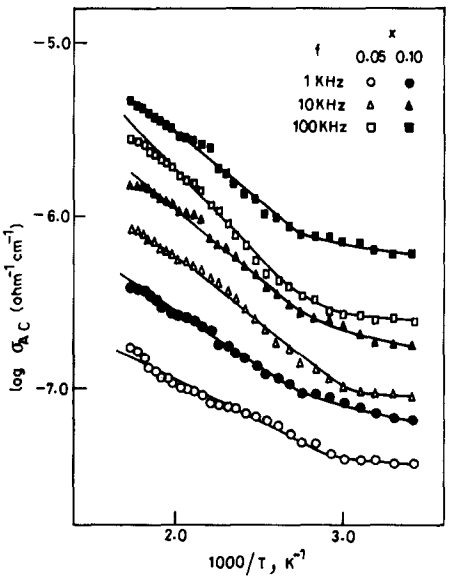

FIG. 4. Variation of log σ_{AC} with $1000/T$ for samples with $x = 0.05$ and 0.10 in the system $SrTi_{1-x}Mg_xO_{3-x}$.

E_B, and hopping at energies close to it, (ii) hopping of charge carriers at localized levels close to E_F similar to impurity conduction in heavily doped crystalline semiconductors, and (iii) thermally activated rotation of dipoles, i.e., if the material contains dipoles which can point in two or more directions, with energies W_1 and W_2 ($\Delta W = W_1 - W_2$) and with a jump time τ from the lower to the upper state, both ΔW and τ varying over a wide range including zero (*12*).

All three mechanisms predict a frequency dependence of AC conductivity given by Eq. (3) with $s \leq 1$. The last two mechanisms predict that the AC conductivity is proportional to temperature, T. Mechanism (i) predicts the temperature dependence of σ_{AC} as (*12*)

$$\sigma_{AC}(T) \alpha \exp[-(E_F - E_B)/kT]. \quad (4)$$

We have also observed an exponential dependence of σ_{AC} on temperature above 350 K for these samples (Fig. 4). This indicates that the conduction occurs mainly by mechanism (i), i.e., transport by carriers excited into localized states at the band edge, E_B, and hopping at energies close to it. For this mechanism, the temperature and frequency dependence can be expressed by the relation (*13*)

$$\sigma_{AC}(\omega,T) = \frac{\pi^3}{96} e^2 kT[N(E_B)]^2 \alpha^{-5} \omega \left[\ln \frac{\nu_{ph}}{\omega}\right]^4 \times \exp[-(E_F - E_B)/kT], \quad (5)$$

where $N(E_B)$ is the density of states at an energy, E_B, away from the Fermi level, ν_{ph} is characteristic optical phonon frequency, and α^{-1} is the radius of localized wave function. The frequency dependence (given by the above equation) can be written (*12*) in the form of Eq. (3) with

$$s = \frac{d[\ln\{\omega \ln^4(\nu_{ph}/\omega)\}]}{d(\ln \omega)} = 1 - \frac{4}{\ln(\nu_{ph}/\omega)}. \quad (6)$$

At a particular frequency, e.g., $\omega = 10^4/S^{-1}$, s varies from 0.4 to 0.8 for ν_{ph} in the range 10^7–10^{13} Hz. If we assume values of ν_{ph} to be of the order of 10^9–10^{10} Hz for our samples, the value of s would be in the range 0.4–0.6 as obtained by us.

The variation of DC conductivity for mechanism (i) with temperature can be written as (*12*)

$$\sigma = \sigma_1 \exp[-(E_F - E_B + W_1)/kT],$$

where W_1 is the energy for hopping. The difference between the activation energies E_a and E_a' for DC and AC conductivity, respectively, is the activation energy, W_1, for hopping among the localized levels at the band edge, E_B. The value of W_1 is almost the same for both samples (Table II).

Although the conductivity behavior can be explained by mechanism (i), mechanism (iii) also contributes to the AC conductivity. This contribution is due to formation of associated Mg^{2+}–oxygen vacancy defect pairs forming dipoles. These dipoles can change their orientation by the jumping of oxygen ions into neighboring oxygen vacancies. Because of random distribution of Mg^{2+} ions and oxygen vacancies, the associated defect pairs may be separated by varying distances giving rise to a range of ΔW and τ values as described for mechanism (iii).

Dielectric Behavior

Variation of dielectric constant, ε_r, with temperature at 1, 10, and 100 kHz for x = 0.00, 0.01, 0.05, and 0.10 is shown in Figs. 5, 6, 7, and 8, respectively. Behavior of samples x = 0.05 and 0.10 is similar and different from that of x = 0.00 and 0.01. For $SrTiO_3$ (x = 0.00), there is very little decrease of dielectric constant with temperature up to 400 K and thereafter it increases very rapidly with temperature. Variation of ε_r with temperature decreases with increasing frequency and ε_r becomes almost independent of temperature at 100 kHz. For the

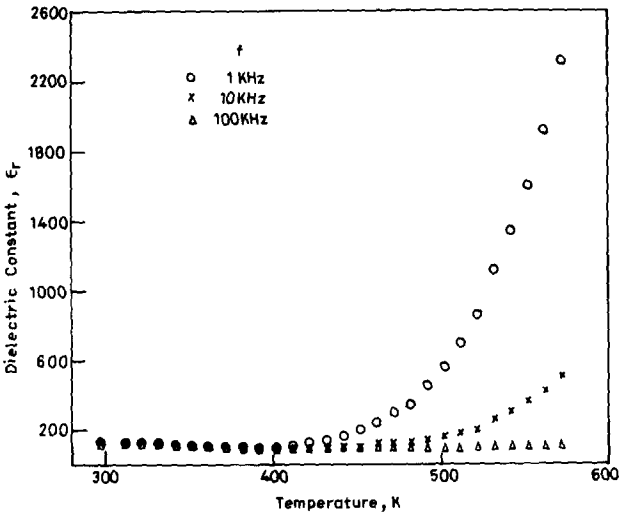

FIG. 5. Variation of dielectric constant, ε_r, with temperature for $SrTiO_3$.

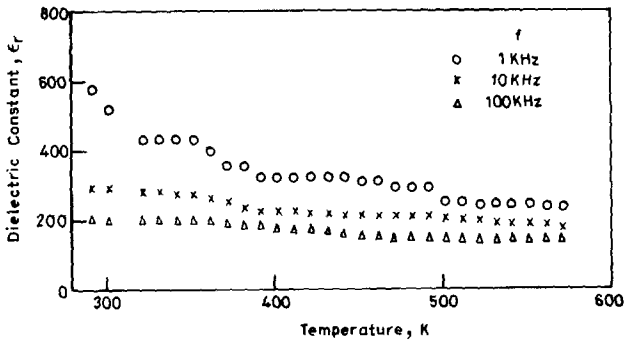

FIG. 6. Variation of dielectric constant, ε_r, with temperature for $SrTi_{0.99}Mg_{0.01}O_{2.99}$.

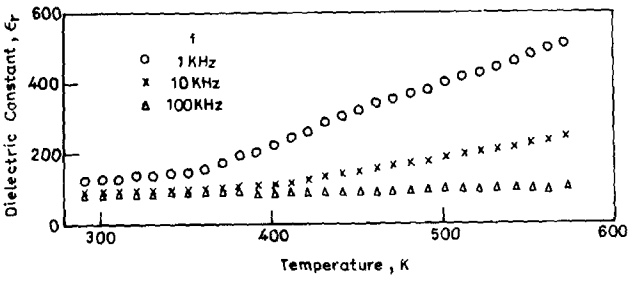

FIG. 7. Variation of dielectric constant, ε_r, with temperature for $SrTi_{0.95}Mg_{0.05}O_{2.95}$.

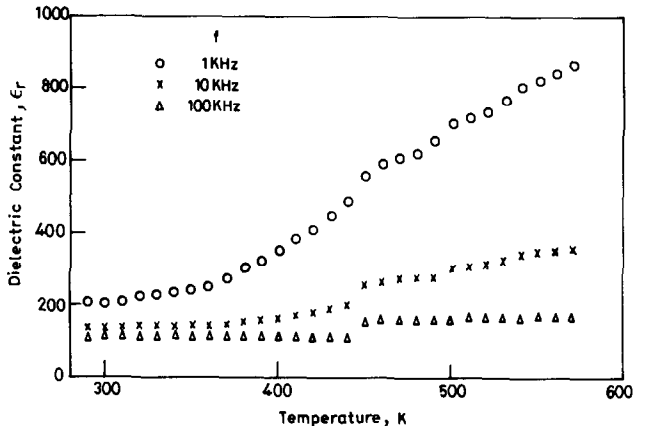

FIG. 8. Variation of dielectric constant, ε_r, with temperature for $SrTi_{0.90}Mg_{0.10}O_{2.90}$.

$x = 0.01$ sample, ε_r decreases with temperature. The temperature variation of ε_r decreases with increasing frequency just like $SrTiO_3$. It differs from $SrTiO_3$ in that there is no sharp increase in ε_r with T after 400 K. Figures 7 and 8 show that for $x = 0.05$ and 0.10, ε_r remains almost independent of temperature up to a particular temperature, T_c. Above T_c it increases linearly with temperature. T_c shifts to higher values with increasing frequency. Further ε_r decreases with increasing frequency in both samples. Plots of log ε_r with log f at two temperatures are shown in Fig. 9. These plots are linear. Thus variation of ε_r with temperature and frequency can be expressed by the relation

$$\varepsilon_r = A(T - T_c)\omega^{-s'}, \qquad (7)$$

where A is a constant. The values of s' are close to 0.3 and slightly increase with temperature.

The dielectric behavior of these samples can be understood in light of the presence of associated Mg^{2+}–oxygen vacancy pairs which constitute dipoles as mentioned earlier. These defect pairs may be separated by varying distances. These dipoles may not be able to respond to external field at low temperatures (below T_c) due to lower mobility of O^{2-} ions. Above T_c, different dipoles may start orienting with the external field contributing to the polarization and thus leading to observed increase in ε_r. The observed increase in ε_r above T_c may also be partly due to interfacial polarization which arises due to random distribution of Mg^{2+} ions in the lattice. Presence of the dipoles (defect pairs) and chemical inhomogeneities in these two compositions also accounts for frequency dependence of ε_r. Dis-

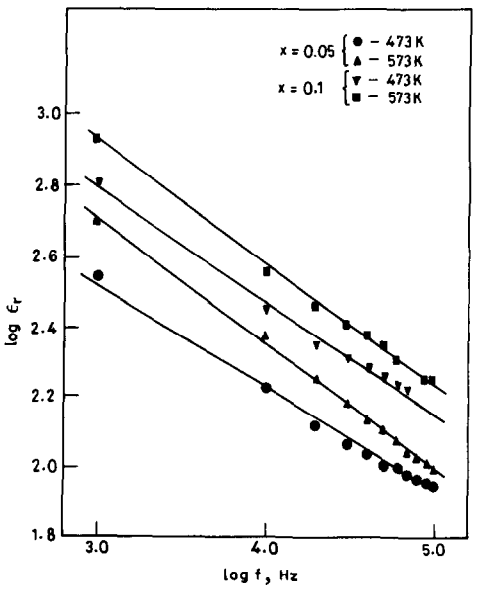

FIG. 9. Variation of log ε_r with log f for the system $SrTi_{1-x}Mg_xO_{3-x}$.

persion of ε_r at low temperatures in $x = 0.01$ may also be due to random distribution of Mg^{2+} ions in it. Dielectric loss, tan δ, in all compositions is high, being maximum in $x = 0.01$. This is in accordance with the highest conductivity observed in this sample. The tan δ decreases with increasing frequency in all samples at all temperatures, indicating that loss is predominantly due to conductivity.

Acknowledgment

The authors are thankful to the Department of Science and Technology, Government of India, for financial support.

References

1. G. L. Skanvi and E. N. Matveena, *Sov. Phys.* **3,** 905 (1957).
2. R. M. Glaister and J. W. Woodner, *J. Electron. Control* **6,** 385 (1959).
3. T. Y. Tien and L. E. Cross, *Japan. J. Appl. Phys.* **6,** 459 (1967).
4. J. Bouwma, K. J. DeVries, and A. J. Burgraaf, *Phys. Status Solidi A* **35,** 281 (1976).
5. I. Burn and S. Neirman, *J. Mater. Sci.* **17,** 1982 (1984).
6. S. Waku, *N.T.T. Res. Appl. Rep.* **16,** 975 (1967).
7. N. Yamaoka, *Bull. Amer. Ceram. Soc.* **65,** 1149 (1986).
8. B. Jaffe, W. R. Cook, Jr., and H. Jaffe, *in* "Piezoelectric Ceramics," Chap. 10, Academic Press, New York/London (1971).
9. K. W. Browall, O. Muller, and R. H. Doremus, *Mater. Res. Bull.* **11,** 1475 (1976).
10. D. P. Karim and A. T. Aldred, *Phys. Rev. B* **20,** 2255 (1979).
11. G. V. Subbarao, B. M. Wanklyn, and C. N. R. Rao, *J. Phys. Chem. Solids* **32,** 345 (1971).
12. N. F. Mott and E. A. Davis, *in* "Electronic Processes in Non-crystalline Materials," Chap. 6, Oxford Univ. Press (Clarendon), New York/London (1979).
13. S. R. Elliott, *Philos. Mag. B* **37,** 553 (1978).